

# X-ray structure of human stromelysin catalytic domain complexed with nonpeptide inhibitors: Implications for inhibitor selectivity

ALEXANDER G. PAVLOVSKY,<sup>1</sup> MARK G. WILLIAMS,<sup>3</sup> QI-ZHUANG YE,<sup>2,4</sup>  
DANIEL F. ORTWINE,<sup>1</sup> CLAUDE F. PURCHASE II,<sup>1</sup> ANDREW D. WHITE,<sup>1</sup>  
V. DHANARAJ,<sup>3</sup> BRUCE D. ROTH,<sup>1</sup> LINDA L. JOHNSON,<sup>2</sup> DONALD HUPE,<sup>2</sup>  
CHRISTINE HUMBLET,<sup>1</sup> AND TOM L. BLUNDELL<sup>3</sup>

<sup>1</sup>Department of Chemistry, Parke-Davis Pharmaceutical Research, Division of Warner-Lambert Company, Ann Arbor, Michigan 48105

<sup>2</sup>Department of Biochemistry, Parke-Davis Pharmaceutical Research, Division of Warner-Lambert Company, Ann Arbor, Michigan 48105

<sup>3</sup>Department of Biochemistry, University of Cambridge, Cambridge CB2 1QW, United Kingdom

(RECEIVED November 3, 1998; ACCEPTED January 26, 1999)

## Abstract

Effective inhibitors of matrix metalloproteinases (MMPs), a family of connective tissue-degrading enzymes, could be useful for the treatment of diseases such as cancer, multiple sclerosis, and arthritis. Many of the known MMP inhibitors are derived from peptide substrates, with high potency *in vitro* but little selectivity among MMPs and poor bioavailability. We have discovered nonpeptidic MMP inhibitors with improved properties, and report here the crystal structures of human stromelysin-1 catalytic domain (SCD) complexed with four of these inhibitors. The structures were determined and refined at resolutions ranging from 1.64 to 2.0 Å. Each inhibitor binds in the active site of SCD such that a bulky diphenyl piperidine moiety penetrates a deep, predominantly hydrophobic S<sub>1</sub>' pocket. The active site structure of the SCD is similar in all four inhibitor complexes, but differs substantially from the peptide hydroxamate complex, which has a smaller side chain bound in the S<sub>1</sub>' pocket. The largest differences occur in the loop forming the "top" of this pocket. The occupation of these nonpeptidic inhibitors in the S<sub>1</sub>' pocket provides a structural basis to explain their selectivity among MMPs. An analysis of the unique binding mode predicts structural modifications to design improved MMP inhibitors.

**Keywords:** drug design; matrix metalloproteinase; MMP-3; nonpeptide inhibitors; X-ray crystallography

Matrix metalloproteinases (MMPs) are a family of zinc-dependent, matrix-degrading endopeptidases that include collagenases, gelatinases, and stromelysins (Woessner, 1991). Connective tissue remodeling is a continuous process required for normal physiological events such as angiogenesis, wound healing, and fetal development. However, uncontrolled matrix degradation may result in diseases such as cancer, multiple sclerosis, and arthritis (Nagase, 1996; Steinman, 1996; Stetler-Stevenson et al., 1996). Consequently, MMP activity is tightly regulated at several levels of expression and activation. Developing effective MMP inhibitors to modulate MMP activity is one approach to treat these degenerative diseases (White et al., 1997a).

Potent MMP inhibitors have been developed by modifying the natural substrates of these enzymes. These peptide-derived inhibitors usually contain a zinc chelating group such as carboxylate, hydroxamate, phosphonate, or phosphinate (Morphy et al., 1995). The binding modes for some of these inhibitors have been revealed in X-ray crystal and NMR solution structures of the enzyme/inhibitor complexes (Lovejoy et al., 1994a, 1994b; Stams et al., 1994; Becker et al., 1995; Browner et al., 1995; Van Doren et al., 1995; Dhanaraj et al., 1996). In all of these structures, the chelating group interacts with the catalytic zinc as a monodentate or bidentate ligand, while the peptide moiety occupies the active site groove on either the prime or nonprime side. The zinc chelation and hydrogen-bond network, as well as other interactions, explain the high potency *in vitro*. However, in general, these inhibitors show little selectivity among MMP family members. A group of peptide hydroxamates with P<sub>1</sub>' residues of varying sizes have shown selectivity for gelatinase A (Porter et al., 1994), indicating that variations in the size and hydrophobicity of the S<sub>1</sub>' pocket may allow

Reprint requests to: Alexander G. Pavlovsky, Department of Chemistry, Parke-Davis Pharmaceutical Research, Division of Warner-Lambert Company, Ann Arbor, Michigan 48105; e-mail: Alexander.Pavlovsky@wl.com.

<sup>4</sup>Current address: Shanghai Institute of Materia Medica, Chinese Academy of Sciences, Shanghai, People's Republic of China 200031.

exploitation for selectivity (Stams et al., 1994). In a recent NMR study of stromelysin/nonpeptide hydroxamic acid inhibitor complexes (Olejniczak et al., 1997), it was shown that a large hydrophobic biphenyl side chain within the inhibitor could be accommodated in the  $S_1'$  pocket.

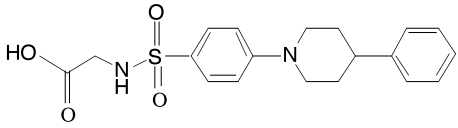
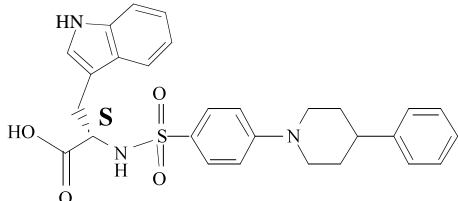
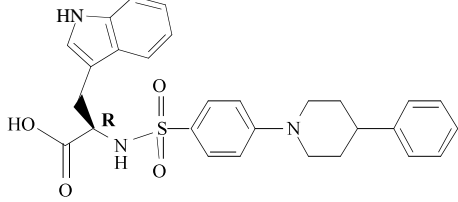
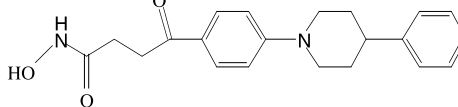
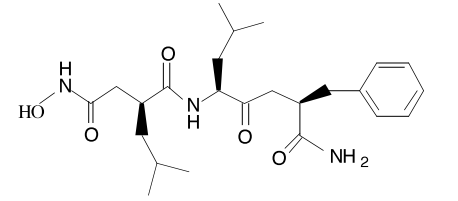
Through mass screening and subsequent synthetic modification of the hits, we have recently discovered nonpeptidic MMP inhibitors selective for human stromelysin-1 (I–IV, Table 1) (Ortwin et al., 1997; White et al., 1997b). The X-ray crystal structures of the enzyme/inhibitor complexes show a unique inhibitor binding mode in the  $S_1'$  pocket that can be used to rationalize the observed selectivity. The detailed structural information can be used to support the observed in vitro activity profiles and to help guide the design of second generation MMP inhibitors with improved potency and selectivity.

## Results and discussion

### Overall structure

Four different crystal forms (hexagonal, monoclinic, and two tetragonal) were obtained while crystallizing SCD with nonpeptide

**Table 1.** Inhibitors cocrystallized with SCD

Number	Structure	$K_i$ (nM)
I		14
II		19
III		36
IV		15
TPH <sup>a</sup>		13

<sup>a</sup>Tripeptide hydroxamate inhibitor described in Dhanaraj et al. (1996).

inhibitors. Although the space groups in the case of the tetragonal crystals are identical and the unit cell dimensions are similar (Table 2), crystals of SCD with inhibitors I, II, and IV have different packing than those with inhibitor III.

The protein folding of SCD observed in these inhibitor complexes is very similar to that found in the complex of SCD with a peptide hydroxamate (Dhanaraj et al., 1996) (Fig. 1). It can be described as an open-face sandwich with  $\alpha$ - $\beta$  topology, three  $\alpha$ -helices, and a twisted five-stranded  $\beta$ -sheet. It is very similar to the structures of other MMPs. The second helix, helix B, forms the bottom of the active site, and the two active site walls are formed by the fourth  $\beta$ -strand on one side and the N-terminal fragment and the loop connecting helices B and C on the other side. The catalytic zinc (Zn1) is located in the center of the active site cleft. Two histidines donated by helix B (His201, His205) and a third one from the loop between the B and C helices (His211) chelate the catalytic zinc. In the sulfonamide structures, the fourth ligand comes from the carboxyl oxygen of the inhibitor bound in the active site. In the hydroxamide inhibitor complex, two of the inhibitor oxygen atoms (carbonyl and hydroxyl) provide the fourth and fifth ligands for Zn1.

An additional seven-amino acid fragment at the amino terminus of SCD (residues 83–89) was found in all four SCD complexes reported here. The main-chain groups and side chains of all seven residues are very well ordered except for the side chain of Arg84, which is disordered beyond the  $C\beta$  atom. Residues 83 through 86 have a  $\beta$ -strand conformation while residues 86 through 89 form a type II  $\beta$ -turn. The conformation of the heptapeptide N-terminal fragment is stabilized by seven hydrogen bonds and the charge interaction between the N-terminal amino group and the Asp237 carboxylate. This is very similar to other reported SCD/inhibitor complexes (Becker et al., 1995; Finzel et al., 1998). Despite the fact that the same protein was used for cocrystallization with both the peptide hydroxamate and nonpeptide inhibitors, this heptapeptide fragment was not observed in the hydroxamate complex (Dhanaraj et al., 1996).

In every tetragonal crystal, a sulfate ion was found at a unique position on the diagonal crystallographic dyad. This sulfate spans the amino terminus of the first  $\alpha$ -helix (residues 110–125) with the symmetry-related copy. In addition to the dipole interactions, the two sulfate oxygen atoms are engaged in three hydrogen bonds with  $N\epsilon$  of Lys110, its main-chain amino group, and a proximal water molecule. Apparently, the sulfate found in the tetragonal crystal forms is an artifact of crystallization. Sulfate is not present in the hexagonal or monoclinic crystals of the complex of SCD with the hydroxamide inhibitor IV, although they were grown under the same conditions as the tetragonal crystals (form 1 in Table 2).

The structural zinc (Zn2) and two of the bound calciums (Ca1–2) are included in the model as reported elsewhere (Becker et al., 1995; Dhanaraj et al., 1996; Finzel et al., 1998). Ca3 forms an unusual trigonal bipyramidal coordination. The carboxyl oxygens of Asp182, Glu184, and a water molecule oxygen atom form the triangle with Ca3 in the center, and the Asp107 carboxyl and Asp182 carbonyl oxygen atoms are located at the top and bottom of the bipyramid. This coordination is quite rare for calcium; only one example with a Ca ion in a similar geometry was found in the literature (Ca2 in the structure of subtilisin Carlsberg complex with eglin (McPhalen et al., 1985) Protein Data Bank (PDB) code 2SEC). The thermal factor of Ca3 is about twice that of the other two calcium ions, which may indicate its lower occupancy.

**Table 2.** Data collection and refinement statistics

	Inhibitor number					
	I	II	III	IV	IV	IV
Inhibitor type	Sulfonamide	Sulfonamide	Sulfonamide	Hydroxamide	Hydroxamide	Hydroxamide
Space group (crystal form)	P4 <sub>1</sub> 2 <sub>1</sub> 2 (1)	P4 <sub>1</sub> 2 <sub>1</sub> 2 (1)	P4 <sub>1</sub> 2 <sub>1</sub> 2 (2)	P6 <sub>5</sub> 22 (3)	P2 <sub>1</sub> (4)	P4 <sub>1</sub> 2 <sub>1</sub> 2 (1)
Unit cell dimensions (Å)	<i>a</i> = <i>b</i> = 70.0, <i>c</i> = 77.7	<i>a</i> = <i>b</i> = 69.9, <i>c</i> = 77.8	<i>a</i> = <i>b</i> = 69.4, <i>c</i> = 74.4	<i>a</i> = <i>b</i> = 80.6, <i>c</i> = 122.7 $\gamma$ = 120.0°	<i>a</i> = 46.9, <i>b</i> = 61.2, <i>c</i> = 74.5, $\beta$ = 92.4°	<i>a</i> = <i>b</i> = 69.9, <i>c</i> = 77.4
Molecules per au.	1	1	1	1	2	1
Data collection						
Maximum resolution (Å)	2.0	1.8	1.64	2.3	2.0	1.7
Resolution in the last shell	2.1–2.0	1.93–1.8	1.7–1.64	2.5–2.3	2.2–2.0	1.9–1.7
Unique reflections (total)	13,572 (142,019)	18,177 (88,271)	20,986 (80,181)	9,112 (40,899)	19,764 (48,592)	20,185 (124,335)
Completeness % (last shell)	99.9 (99.9)	97.5 (98.9)	92.3 (92.4)	80.0 (78.4)	93.0 (92.9)	99.2 (97.6)
<i>R</i> <sub>sym</sub> (last shell)	0.091 (0.34)	0.062 (0.29)	0.038 (0.12)	0.073 (0.30)	0.090 (0.31)	0.057 (0.27)
Refinement statistics						
Resolution range (Å)	8.0–2.0	8.0–1.8	8.0–1.64	8.0–2.3	8.0–2.0	8.0–1.7
Number of reflections ( <i>F</i> > 2σ)	12,936	16,172	20,767	7,689	16,909	19,438
<i>R</i> <sub>f</sub> / <i>R</i> <sub>free</sub> <sup>a</sup>	0.197/0.214	0.194/0.23	0.209/0.245	0.195/0.255	0.209/0.269	0.198/0.218
Number of atoms (waters)	1,454 (86)	1,459 (74)	1,532 (147)	1,418 (82)	2,787 (81)	1,488 (120)
RMSD from ideal						
Bond length (Å)	0.011	0.010	0.009	0.011	0.009	0.012
Bond angles (°)	2.6	2.6	3.1	2.7	2.4	2.6
Torsion angles (°)	27.1	27.3	27.0	27.4	26.8	27.2
Improper angles (°)	2.0	2.2	1.9	2.1	1.8	2.3
Average <i>B</i> -factors (Å <sup>2</sup> )						
Protein/inhibitor/water	19.2/18.0/41.8	18.1/17.8/34.0	11.5/14.6/30.0	29.1/20.2/55.3	15.7/10.8/33.5	16.8/13.8/40.0

<sup>a</sup> $R_f = \sum |F_{obs} - F_{calc}| / \sum F_{obs}$ ,  $R_{free}$  is the  $R_f$  for a subset of 10% of the reflections excluded from the crystallographic refinement.

### Inhibitor binding

All four nonpeptide inhibitors are bound in the SCD active site close to the catalytic zinc. The binding mode is similar for each, with the diphenylpiperidine side chain occupying the S<sub>1</sub>' pocket. Every inhibitor is tightly bound, as indicated by the low thermal atomic parameters (Table 2). Analyses of the high-resolution electron density (Fig. 2) are consistent with a pseudo-chair conformation of the inhibitor piperidine group containing a largely trigonal planar ring nitrogen. This is similar to what is observed in the Cambridge Structural database (Allen et al., 1983) for related small molecules.

Three types of interactions stabilize inhibitor binding in the active site of SCD: catalytic zinc ligation (Table 3), hydrogen bonds between inhibitor and protein, and hydrophobic interactions between the diphenyl piperidine side chain and S<sub>1</sub>' pocket residues. With a sulfonamide inhibitor (I, II, and III) bound in the SCD active site, the carbonyl oxygen of the inhibitor interacts with Zn1, creating a near symmetrical tetrahedral configuration. All four ligating atoms belong to the first coordination sphere of Zn1, being 2.0–2.2 Å distant (Table 3). A different Zn1 coordination arrangement is found in the complex of SCD with the hydroxamide inhibitor (IV). This coordination can be described as a distorted

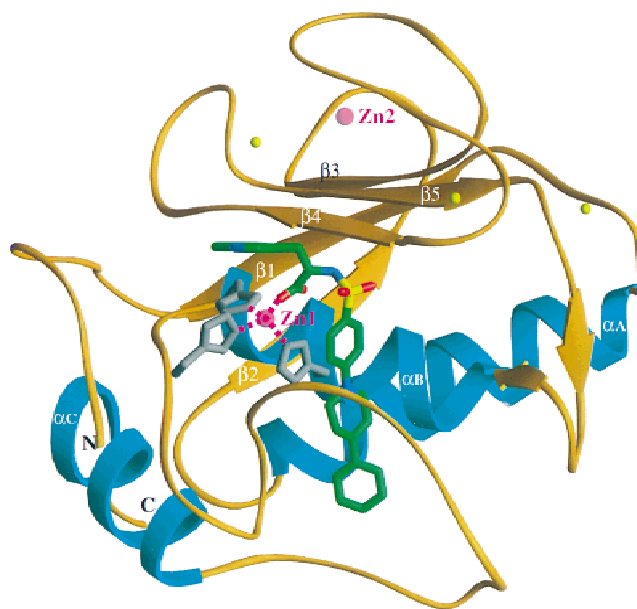


**Fig. 1.** Ribbon (Carson, 1991) representation of the SCD/II inhibitor complex. Zinc and calcium ions are shown as magenta and yellow spheres.

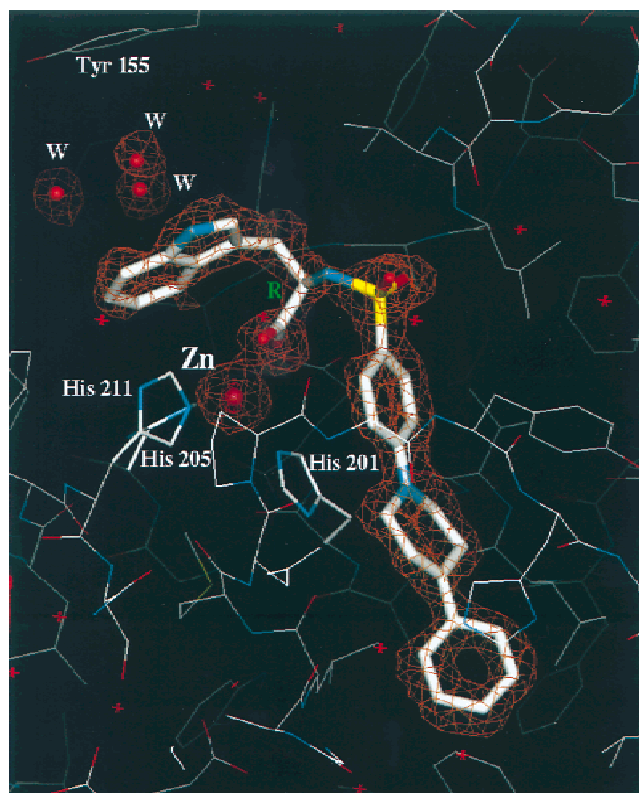


**Fig. 2.**  $2F_o - F_c$  electron density fragment showing inhibitor III bound in SCD active site. Density is contoured at  $1.2\sigma$  level.

trigonal bipyramid, with the five chelating atoms being almost equidistant from Zn1 (Table 3). Ne atoms of His201 and His205, in addition to hydroxyl oxygen of the hydroxamate, form the triangular plane of the bipyramid, with Zn1 at the center. His211 Ne and the carbonyl oxygen of the hydroxamate form the top and bottom. This coordination is very similar to that reported previously for the SCD/peptide hydroxamate inhibitor complex (Becker et al., 1995; Dhanaraj et al., 1996).

In addition to zinc ligation, sulfonamide inhibitors I and II form three hydrogen bonds to SCD. These occur between one of the sulfonyl oxygen atoms and Leu164, the sulfonamide nitrogen of the inhibitor and Ala165, and the inhibitor hydroxyl group and Glu202 O $\epsilon$  (Table 3). When the sulfonamide inhibitor III binds to SCD, only two of these three hydrogen bonds are present. Because the tryptophan amino acid side chain is in the *R*-configuration, the sulfonamide nitrogen points away from the carbonyl oxygen of Ala165 (Fig. 2), and the third hydrogen bond between the inhibitor amine nitrogen and Ala165 O cannot be formed.

The hydroxamate inhibitor IV/SCD complex exhibits a different hydrogen bond pattern. Similar to the sulfonamide inhibitor complexes, there are hydrogen bonds between the inhibitor carbonyl oxygen atom alpha to the aryl group and the Leu164 amine, and between the hydroxamate NH group and backbone carbonyl oxygen of Ala165. An additional hydrogen bond connects the hydroxamate hydroxyl (this is the same hydroxyl that chelates Zn1) and Glu202 O $\epsilon$ 1. Interestingly, in the SCD/TPH complex, the hydroxyl oxygen of the inhibitor is likely to be hydrogen bonded to Glu202 O $\epsilon$ 2, while in SCD/nonpeptide inhibitor complexes, a bond with O $\epsilon$ 1 is more likely (Table 2).

One of the remarkable features of the present inhibitor complexes is the deep penetration of the long diphenyl piperidine side chain into the  $S_1'$  pocket. This pocket is, in fact, an open channel running from the center of the active site near the catalytic zinc to the molecular surface where it is exposed to water. The analogous  $S_1'$  pockets in MMPs such as matrilysin (Browner et al., 1995) and fibroblast collagenase (Borkakoti et al., 1994; Lovejoy et al., 1994a) are much shallower and would not be expected to accommodate a lengthy side chain such as a diphenyl piperidine without significant conformational changes in the protein. The  $S_1'$  channel of SCD is predominantly composed of hydrophobic residues, including the main-chain atoms of Leu197, Val198, Leu218, Tyr220, Pro221 through Ser225, and the side-chain atoms of Leu197, Val198, His201, Leu218, Tyr223, His224, and Leu226. Within the pocket, the imidazole ring of His201 stacks almost perfectly with the proximal phenyl ring of the inhibitor. Another imidazole from His224 forms a loose stack with the distal phenyl ring of the inhibitor at an angle of  $\sim 30^\circ$ . The positions of the diphenyl piperidine in all sulfonamide inhibitors are almost identical. A small difference is seen for the hydroxamate inhibitor IV complex, where the ring system inserts about 0.4 Å deeper into the  $S_1'$  pocket.

Inhibitors II and III are *S* and *R* stereoisomers, respectively, with the chiral center at the tetrahedral  $C\alpha$  atom. Despite different chirality, the indole rings in both complexes are located in the same area of the active site of SCD, the  $S_1$  pocket (Fig. 3). As part of the active site cleft, this pocket is composed of the side chains of Phe86 and Phe210, two of the Zn1-chelating histidines (His205 and His211), and the catalytic zinc as one wall. The other wall contains the side chain of Tyr155, and partially Tyr168. The main-chain atoms of residues 165–168 form the bottom of this pocket. The distance between the Tyr155 phenol and inhibitor indole ring is about 8 Å, resulting in a pocket that is two times wider than that needed to accommodate the inhibitor aromatic ring. The remaining space is filled with three water molecules wedged between the two rings. Because the indole ring of II is somewhat deeper in the  $S_1$  pocket than that for III (average 1.5 Å difference for indole ring atoms), there are corresponding differences in the locations of the space-filling water molecules (Fig. 3).

Filling a shallow  $S_1$  pocket with an indole ring does not seem to be advantageous for inhibitor binding (compare  $K_i$ 's for I and II in Table 1) regardless of its depth. In contrast, loss of a direct inhibitor to protein hydrogen bond reduces potency somewhat. Thus, inhibitor II, which forms three direct hydrogen bonds with the protein, is almost twice as potent as its *R* enantiomer III, which forms two direct hydrogen bonds plus a weak water-mediated hydrogen bond to the carbonyl oxygen of Pro221 on the opposite side of the binding groove.

The previously described binding mode for TPH in the active site of SCD (Dhanaraj et al., 1996) differs significantly from that observed for the nonpeptide inhibitors. The tripeptide inhibitor fills the prime side of the active site cleft, forming an extended peptide strand antiparallel to the 162–165 residue fragment of SCD. An extensive hydrogen bonding network between main-chain atoms of protein and peptide, together with catalytic zinc chelation, provide a tight anchor for the inhibitor (Fig. 4A). Four of the five reported hydrogen bonds are with backbone groups (the fifth bond is with Glu202 O $\epsilon$ 2) (Dhanaraj et al., 1996). Out of three tripeptide inhibitor side chains, leucine in position  $P_1'$  is the only one buried deeply in a specificity pocket. The inhibitor isobutyl and phenyl groups at  $P_2'$  and  $P_3'$  are more solvent exposed and less spatially restricted than the isobutyl at  $P_1'$ . Another reported tripeptide in-

**Table 3.** Hydrogen bonds and catalytic zinc ligation in SCD/inhibitor complexes

Type of interaction	Atoms of		Inhibitor				
	Protein	Inhibitor	I	II	III	IV	TPH <sup>a</sup>
			Distance (Å)				
Hydrogen bond	Asn162 O	HN(P3')	—	—	—	—	2.7
	Phe223 O	O=C(P2')	—	—	—	—	2.9
	Pro221 O	HN(P2')	—	—	—	—	3.0
	Leu164 N	O=C(P1')	—	—	—	—	2.8
	Leu164 N	O=S;O $\alpha^b$	2.8	2.8	2.8	2.8	
	Ala165 O	HN-S	2.9	2.7	—	—	
	Ala165 O	HN	—	—	—	2.8	2.8
	Glu202 Oe1	HO	2.7	2.6	2.6	2.7	3.1
	Glu202 Oe2	HO	3.4	3.2	3.1	3.3	2.8
Zinc ligating	Zn1	O=C	1.8	2.0	2.0	2.2	2.2
	Zn1	OH	—	—	—	2.2	2.2
	His201 N $\epsilon$ Zn1		2.1	2.1	2.2	2.1	2.3
	His205 N $\epsilon$ Zn1		2.1	2.2	2.2	2.2	2.3
	His211 N $\epsilon$ Zn1		2.1	2.2	2.2	2.2	2.2

<sup>a</sup>Tripeptide hydraxamate inhibitor (Dhanaraj et al., 1996).

<sup>b</sup>Carbonyl oxygen alpha to aryl (inhibitor IV).

inhibitor (Becker et al., 1995) binds similarly, although the longer homophenyl group at the P<sub>1</sub>' penetrates more deeply into the S<sub>1</sub>' specificity pocket.

Unlike the peptide, these nonpeptide inhibitors fill a small portion of the active site cleft (Fig. 4B), forming fewer hydrogen bonds with the SCD active site atoms (Table 3). Hydrophobic interactions between the diphenyl piperidine and the protein in the S<sub>1</sub>' pocket are more dominant in determining binding energy.

#### Protein conformational changes

The overall structure of SCD, including its active site, is similar in complexes with the four different nonpeptide inhibitors studied here. RMS differences for the common 160 C $\alpha$  atoms in the protein are less than 0.3 Å between any two complexes, SCD/I-IV. The SCD/sulfonamide complexes are more similar to each other than they are to SCD/TPH. This is reflected in an increase in RMS

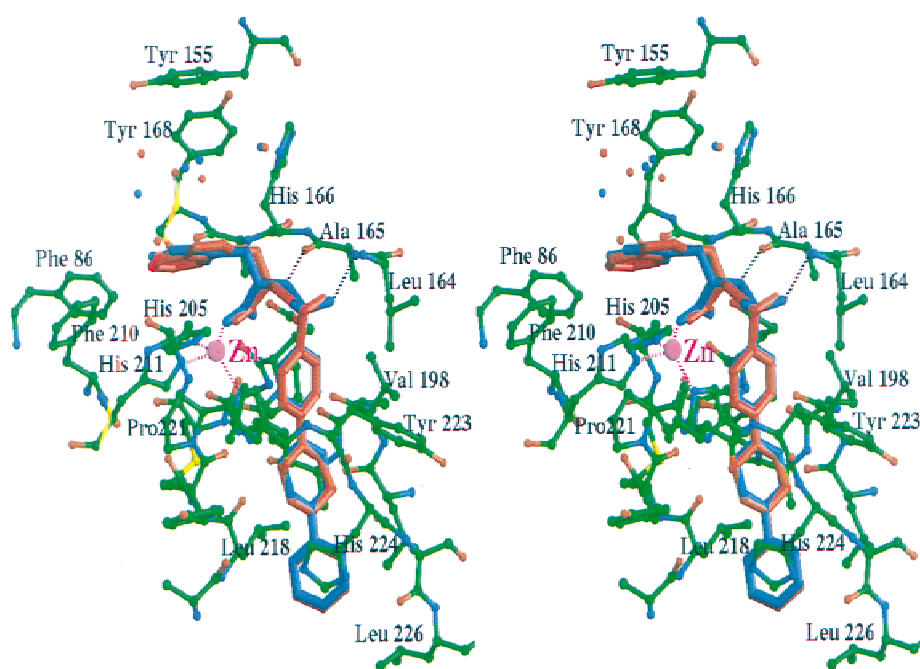


**Fig. 3.** Superposition of inhibitors II (blue) and III (red) in stereo as found in the complexes with SCD. Water molecules in the S<sub>1</sub>' pocket are shown as blue and red spheres.

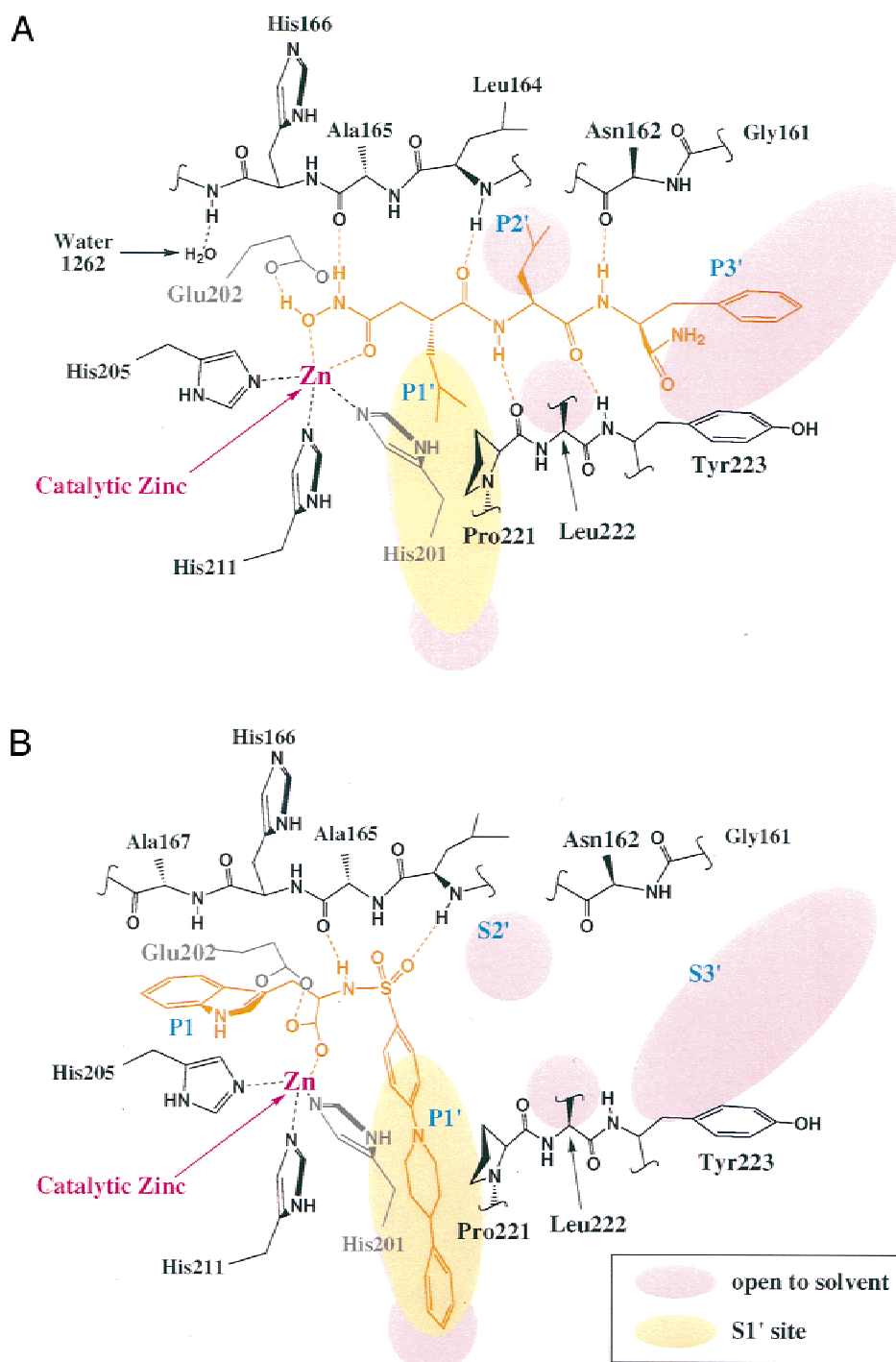


Fig. 4. Schematic diagram of the SCD active site with (A) TPH and (B) II inhibitors bound.

difference for the same 160  $C\alpha$  atoms in common to the SCD/sulfonamide and SCD/TPH complexes. For example, the RMS difference between the SCD/TPH and SCD/III inhibitor complexes is 0.6 Å. One area where protein conformational changes between SCD/peptide and nonpeptide complexes are seen is residues 157–164 in the C-terminal part of the loop connecting  $\beta$ -strands three and four (Fig. 5). Because the longer tripeptide inhibitor occupies the  $S_2'$  and  $S_3'$  subsites, hydrogen bonds are

formed between its backbone and main-chain atoms of Asn162 and Leu164 within this loop (Fig. 4A). These hydrogen bonds have the effect of pulling the loop toward the active site relative to the SCD/nonpeptide complexes (Fig. 4B), where only one inhibitor/protein hydrogen bond is formed (to Leu164), and the subsites  $S_2'$  and  $S_3'$  are vacant.

The most significant conformational changes occur in the area of the  $S_1'$  binding pocket. Residues 212–234 are displaced the most

in response to the diphenyl piperidine binding (the RMS deviation (RMSD) for 23 C $\alpha$  atoms is about 0.8 Å). The largest difference is found for His224. Its C $\alpha$  atom moves 1.4 Å, while its side chain moves more than 2 Å. In the SCD/TPH complex (Dhanaraj et al., 1996) where the S $_1'$  pocket is filled with a relatively small isobutyl group, the His224 N $\epsilon$  is hydrogen bonded directly to Ala217 O. In this conformation, the pocket is too small to accommodate a diphenyl piperidine. Thus, when the nonpeptide inhibitor binds, an opening of the pocket must occur, which results in a shift of His224 followed by a movement of the entire 212–234 loop. In its new position, the His224 imidazole ring is stabilized by hydrogen bonds with the carbonyl oxygen atoms of Thr215 and Ala217, bridged with a tightly bound water molecule (Fig. 5). This water molecule was found in all four SCD/nonpeptide inhibitor complexes.

The fact that the SCD/IV inhibitor complex was crystallized in three crystal forms, and one of them (form 4, Table 2) contained two molecules in the asymmetric unit, allowed us to examine the effect of crystal packing on the conformational stability of the protein. To do this, four crystallographically independent molecules were matched by superposition of their C $\alpha$  atoms. Although the overall differences were small (RMS did not exceed 0.4 Å), there were two local regions with differences larger than average. The loop connecting  $\beta$ -strand four with  $\alpha$ -helix B (residues 186–193) was found to be partially disordered, as was the loop containing residues 212–234. The latter loop is quite flexible and appears to be sensitive to the crystallographic environment. Similar flexibility has been reported for other SCD/nonpeptide complexes (Finzel et al., 1998). The largest conformational differences were observed in two independent molecules of the SCD/IV inhibitor complex in crystal form 3 (Table 2). Crystal packing in one molecule caused this loop to move toward the S $_1'$  channel. As a result, the C $\alpha$  atom of His224 shifted 0.9 Å compared to its position in the second molecule, where this loop was not affected by

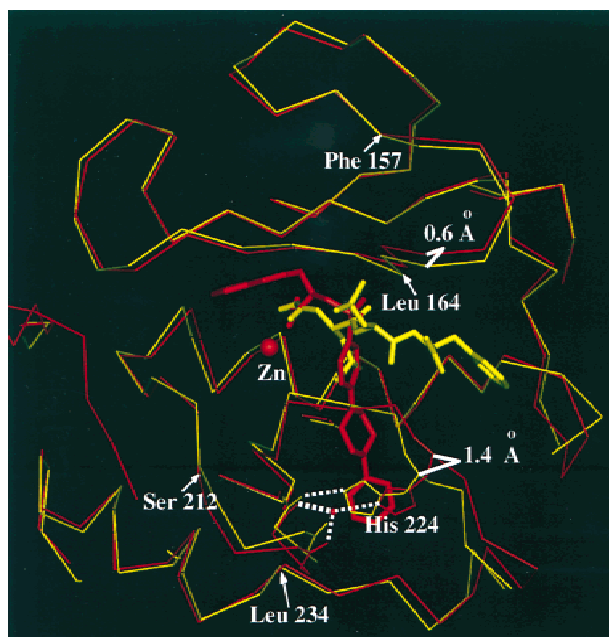


**Fig. 5.** Superposition of the SCD/TPH (yellow) and SCD/III (red) complexes, showing differences in the active site structures.

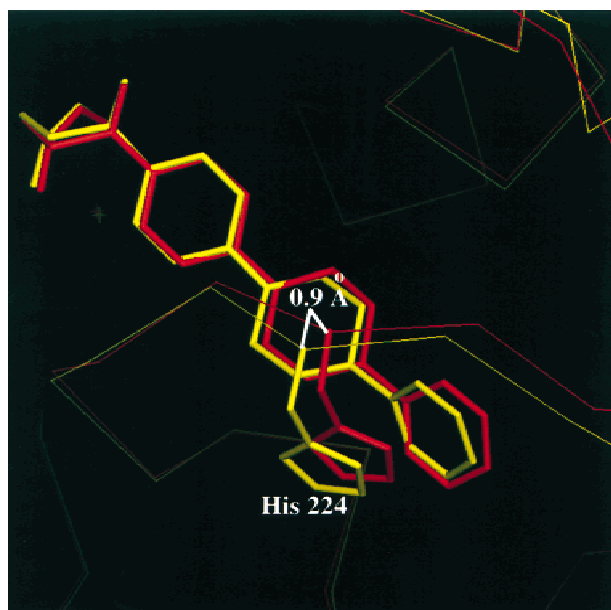


**Fig. 6.** Differences in His224 and inhibitor positions observed in two independent molecules of SCD/IV complex in crystal form 4.

crystal packing. The His224 imidazole, in turn, induces changes in the orientation of the distal phenyl and piperidine rings within the inhibitor (Fig. 6). These changes are smaller for the proximal phenyl ring, and almost undetectable for the rest of the inhibitor.

## Conclusions

Using high-resolution X-ray crystallography, a novel binding mode of four potent, nonpeptide inhibitors in the active site of stromelysin catalytic domain has been characterized. These inhibitors bind differently than peptide-based inhibitors. An extensive network of hydrogen bonds and chelation of the catalytic zinc stabilize the latter in the active site. Hydrophobic interactions in the specificity pockets play a relatively minor role in binding energy. In the presence of nonpeptide inhibitors, loss of binding energy due to a reduced number of hydrogen bonds is compensated by significant hydrophobic interactions between the tricyclic inhibitor side chain and atoms of S $_1'$  recognition channel. These hydrophobic interactions are the defining characteristic for the SCD/inhibitor complexes described here.

These results elucidate fine details of complex formation between the stromelysin catalytic domain and diphenyl piperidine containing inhibitors, and have proven useful in the process of designing more potent and selective inhibitors for stromelysin, which will be discussed in future publications from our laboratories.

## Materials and methods

### Crystallization

Aqueous protein solution was mixed with a three- to fivefold excess of inhibitor, dissolved in DMSO prior to crystallization, and concentrated in a 10 kD centricon. Cocrystals of SCD/inhibitor complexes were grown using the vapor diffusion technique in

5–10  $\mu\text{L}$  hanging/sitting drops containing 0.5–1 mM protein/inhibitor complex, 10–15% PEG 8K, 0.05 M ammonium sulfate, and 0.05 M Na cacodylate buffer (pH 6.5). Drops were equilibrated against 20–30% PEG 8K, 0.1 M ammonium sulfate, and 0.1 M of the same buffer. Often, crystals of  $\text{CaSO}_4$  appeared after several days, and small tetragonal crystals started to grow a week or two later. Complex crystals reached a maximum size of  $0.5 \times 0.3 \times 0.2 \text{ mm}^3$  within a month. The SCD/IV inhibitor complex crystallized in three different forms using the same crystallization conditions. Large hexagonal bipyramid crystals grew first. Two months later, small thin platelets grew in the same drop. Tetragonal crystals were forced to grow by macroseeding with small crystals of SCD/I inhibitor complex.

#### Data collection

Cocrystals of SCD with inhibitors I, II, and IV were mounted into a glass capillary for data collection at room temperature on a MAR Research 300 mm image plate, equipped with a Rigaku-200B rotating anode generator and a graphite monochromator. Diffraction data were processed using XDS (Kabsch, 1988). A crystal of the SCD/III complex was flash-frozen in a low temperature nitrogen stream (temperature  $\sim 190^\circ\text{C}$ ), and data were collected on the same MAR image plate using an X-ray beam focused with a two mirrors system. Diffraction data were processed by DENZO (Otwinowski & Minor, 1997) and scaled by SCALEPACK. Data collection and refinement statistics are summarized in Table 2.

#### Structure determination and refinement

Initial structural solutions for SCD complexes with I and III and hexagonal and monoclinic crystal forms of IV were found by molecular replacement. Unambiguous solutions were obtained by AMoRe software (Navaza, 1994). The protein model, taken from the crystal structure of SCD with a hydroxamate inhibitor (Dhanaraj et al., 1996), was used as a probe. The model included all residues from 90–249, including side chains. Interestingly, although the SCD/III inhibitor complex crystallized in the tetragonal space group and had similar unit cell dimensions as the other tetragonal crystals, it formed a different crystal packing.

For each complex, conventional X-PLOR refinement (Brünger, 1992), alternated with manual adjustment of the model and water molecule locations, was done prior to incorporation of inhibitor.

The atomic coordinates for the three complexes SCD/I–III have been deposited in the PDB (Bernstein et al., 1977) as PDB-ID 1b8y, 1caq, and 1ciz, respectively.

#### References

Allen FH, Kennard O, Taylor R. 1983. Systematic analysis of structural data as a research technique in organic chemistry. *Acc Chem Res* 16:146–153.  
 Becker JW, Marcy AI, Rokosz LL, Axel MG, Burbaum JJ, Fitzgerald PM, Cameron PM, Esser CK, Hagmann WK, Hermes JD, Springer JP. 1995. Stromelysin-1: Three-dimensional structure of the inhibited catalytic domain and of the C-truncated proenzyme. *Protein Sci* 4:1966–1976.  
 Bernstein FC, Koetzle TF, Williams GJB, Meyer EF Jr, Brice MD, Rodgers JR, Kennard O, Shimanouchi T, Tasumi M. 1977. The Protein Data Bank: A

computer-based archival file for macromolecular structures. *J Mol Biol* 112:535–542.  
 Borkakoti N, Winkler FK, Williams DH, D'Arcy A, Broadhurst MJ, Brown PA, Johnson WH, Murray EJ. 1994. Structure of the catalytic domain of human fibroblast collagenase complexed with an inhibitor. *Nat Struct Biol* 1:106–110.  
 Browner MF, Smith WW, Castelhano AL. 1995. Matrilysin-inhibitor complexes: Common themes among metalloproteinases. *Biochemistry* 34:6602–6610.  
 Brünger AT. 1992. *X-PLOR version 3.1, a system for X-ray crystallography and NMR*. New Haven, Connecticut: Yale University Press.  
 Carson M. 1991. RIBBONS 2.0. *J Appl Crystallogr* 24:958–961.  
 Dhanaraj V, Ye Q-Z, Johnson LL, Hupe DJ, Ortwine DF, Dunbar JB, Rubin JR, Pavlovsky A, Humblet C, Blundell TL. 1996. X-ray structure of stromelysin catalytic domain and its comparison with members of the zinc metalloproteinase superfamily. *Structure* 4:375–386.  
 Finzel BC, Baldwin ET, Bryant GL Jr, Hess GF, Wilks JW, Trepod CM, Mott JE, Marshall VP, Petzold GL, Pooman RA, O'Sullivan TJ, Schostarez HJ, Mitchell MA. 1998. Structural characterizations of nonpeptidic thiazazole inhibitors of matrix metalloproteinases reveal the basis for stromelysin selectivity. *Protein Sci* 7:2118–2126.  
 Kabsch WJ. 1988. Evaluation of single-crystal X-ray diffraction data from a position sensitive detector. *J Appl Crystallogr* 21:916–924.  
 Lovejoy B, Cleasby A, Hassell AM, Longley K, Luther MA, Weigl D, McGeehan G, McElroy AB, Drewry D, Lambert MH, Jordan SR. 1994a. Structure of the catalytic domain of fibroblast collagenase complexed with an inhibitor. *Science* 263:375–377.  
 Lovejoy B, Hassell AM, Luther MA, Weigl D, Jordan SR. 1994b. Structure of the catalytic domain of fibroblast collagenase complexed to itself. *Biochemistry* 33:8207–8217.  
 McPhalen CA, Schnebli HP, James MNG. 1985. Crystal and molecular structure of the inhibitor eglin from leeches in complex with subtilisin Carlsberg. *FEBS Lett* 188:55–58.  
 Morphy JR, Millican TA, Porter JR. 1995. Matrix metalloproteinase inhibitors: Current status. *Curr Med Chem* 2:743–762.  
 Nagase H. 1996. Matrix metalloproteinases. In: Hooper N, ed. *Zinc metalloproteinases in health and disease*. London: Taylor and Francis. pp 153–204.  
 Navaza J. 1994. AMoRe: An automated package for molecular replacement. *Acta Crystallogr A* 50:157–163.  
 Olejniczak ET, Hajduk PJ, Marcotte PA, Nettlesheim DG, Meadows RP, Edalji R, Holzman TF, Fesik ST. 1997. Stromelysin inhibitors designed from weakly bound fragments: Effect of linking and cooperativity. *J Am Chem Soc* 119:5828–5832.  
 Ortwine DF, Dhanaraj V, Dunbar JB Jr, Johnson LL, Pavlovsky A, Purchase CF II, White AD, Ye Q-Z. 1997. Structure based design of matrix metalloproteinase inhibitors: What have the structure taught us? Abstract of ACS National Meeting, Las Vegas, Nevada, September, COMP186.  
 Otwinowski Z, Minor W. 1997. Processing of X-ray diffraction data collected in oscillation mode. *Methods Enzymol* 276:307–326.  
 Porter JR, Beeley NRA, Boyce B, Mason B, Millican A, Millar K, Leonard J, Morphy JR, O'Connell JP. 1994. Potent and selective inhibitors of gelatinase-A. 1. Hydroxamic acid derivatives. *Bioorg Med Chem Lett* 4:2741–2746.  
 Stams T, Spurlino JC, Smith DL, Wahl RC, Ho TF, Qoronfleh W, Banks TM, Rubin B. 1994. Structure of human neutrophil collagenase reveals large S<sub>1</sub> specificity pocket. *Nat Struct Biol* 1:119–123.  
 Steinman L. 1996. Multiple sclerosis: A coordinated immunological attack against myelin in the central nervous system. *Cell* 85:299–302.  
 Stetler-Stevenson WG, Hewitt R, Corcoran M. 1996. Matrix metalloproteinases and tumor invasion: From correlation and causality to the clinic. *Cancer Biol* 7:147–154.  
 Van Doren S, Kurochkin A, Hu W, Ye Q-Z, Johnson LL, Hupe D, Zuiderweg E. 1995. Solution structure of the catalytic domain of human stromelysin complexed with a hydrophobic inhibitor. *Protein Sci* 4:2487–2498.  
 White AD, Bocan TMA, Boxer PA, Peterson JT, Schrier D. 1997a. Emerging therapeutic advances for the development of second generation matrix metalloproteinase inhibitors. *Curr Pharm Des* 3:45–58.  
 White AD, Purchase CF II, Baragi V, Finkel M, Hallak H, Hupe D, Johnson LL, Kindt EK, Laemont K, Ortwine DF, Pavlovsky A, Renkiewicz RR, Roth BD, Schrier DJ, Ye Q-Z. 1997b. Selective non-peptide inhibitor of matrix metalloproteinases. Abstract of ACS National Meeting, Las Vegas, Nevada, September, MEDI 110.  
 Woessner JF. 1991. Matrix metalloproteinases and their inhibitors in connective tissue remodeling. *FASEB J* 5:2145–2154.